THE JOURNAL OF PHYSICAL CHEMISTRY LETTERS
A JOURNAL OF THE AMERICAN CHEMICAL SOCIETY

pubs.acs.org/JPCL

Letter

Hopping Behavior Mediates the Anomalous Confined Diffusion of Nanoparticles in Porous Hydrogels

Chundong Xue, Yirong Huang, Xu Zheng,* and Guoqing Hu*

Cite This: *J. Phys. Chem. Lett.* 2022, 13, 10612−10620

Read Online

ACCESS | Metrics & More | Article Recommendations | Supporting Information

ABSTRACT: Diffusion is an essential means of mass transport in porous materials such as hydrogels, which are appealing in various biomedical applications. Herein, we investigate the diffusive motion of nanoparticles (NPs) in porous hydrogels to provide a microscopic view of confined diffusion. Based on the mean square displacement from particle tracking experiments, we elucidate the anomalous diffusion dynamics of the embedded NPs and reveal the heterogeneous pore structures in hydrogels. The results demonstrate that diffusive NPs can intermittently escape from single pores through void connective pathways and exhibit non-Gaussian displacement probability distribution. We simulate this scenario using the Monte Carlo method and clarify the existence of hopping events in porous diffusion. The resultant anomalous diffusion can be fully depicted by combining the hopping mechanism and the hydrodynamic effect. Our results highlight the hopping behavior through the connective pathways and establish a hybrid model to predict NP transport in porous environments.

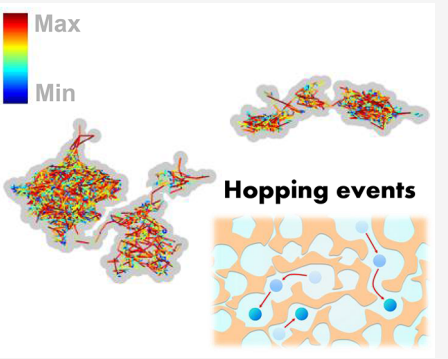

Hydrogels are three-dimensional networks composed of cross-linked polymer chains. Due to their high water content, hydrogels usually show excellent biocompatibility and flexibility similar to natural tissues. Hydrogels have been applied in many biomedical applications such as controlled drug delivery,[1−3] tissue engineering,[4,5] cell culture,[6,7] biosensors,[8,9] and wound healing.[10,11] The porous microstructures of hydrogels make them good materials for transporting biomolecules such as protein therapeutics[12,13] and growth factors.[14] By tuning their physicochemical properties, hydrogels can serve as platforms for the release of therapeutic agents with spatial and temporal control.[4,6,15−19] One essential mechanism underlying the aforementioned applications of hydrogels is related to the hindered mass transport in porous materials. The highly heterogeneous hydrogel environment makes the motion of embedded nanoparticles (NPs) difficult to predict. While similar problems in cancer therapeutics and water filtration have been studied for many years,[1,15,20−23] there is no universal theory that can quantitatively describe particle transport and flow behavior in porous networks.

There are two major challenges. The first is the accurate characterization of the heterogeneous spatial structures in porous networks and the complex pathways for NPs to pass through.[20,24−26] The size of the hydrogel pore is theoretically considered to be the key factor determining the movement of entrapped NPs, whereas the "pore throat" formed by the nonuniform hydrogel microstructure largely limits the transport of NPs. Previous theoretical models based on the average pore size or porosity are too idealized or empirical for practical application.[20,24,27] Atomic force microscopy, nuclear magnetic resonance spectroscopy, and light/X-ray scattering experiments have been performed to detect and describe the porosity.[28,29] However, most of these studies provided only the average pore size and constructed the porosity distribution based on a presumed random distribution due to the lack of dynamic information about the transported NPs and the absence of fluid hydrodynamics.[20,24] The second challenge is to precisely interpret the anomalous diffusive behavior of NPs within confined heterogeneous networks. The Péclet number (Pe), which describes the relative importance of advection versus diffusion, is smaller than unity for NP transport in hydrogels ($Pe = UL/D \sim 0.1$, where U, L, and D are the velocity, length, and diffusion coefficient, respectively); thus, diffusion plays a dominant role in NP transport in hydrogels. Anomalous dynamics have attracted considerable attention in recent years[30−35] and created challenges in extending theories for isotropic media to heterogeneous ones.

The diffusive motion of NPs is hindered in porous media, often resulting in a subdiffusive mean square displacement (MSD).[27,32,34,35] NPs in solid matrices usually diffuse more slowly than those in the bulk due to hydrodynamic damping. The porous structure can significantly influence the MSD behavior: if the NP's percolating path is blocked, the MSD should saturate to a constant value in the long-time limit.[36,37]

Received: September 4, 2022
Accepted: November 7, 2022
Published: November 9, 2022

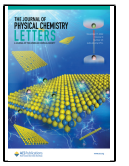

https://doi.org/10.1021/acs.jpclett.2c02733
J. Phys. Chem. Lett. 2022, 13, 10612−10620

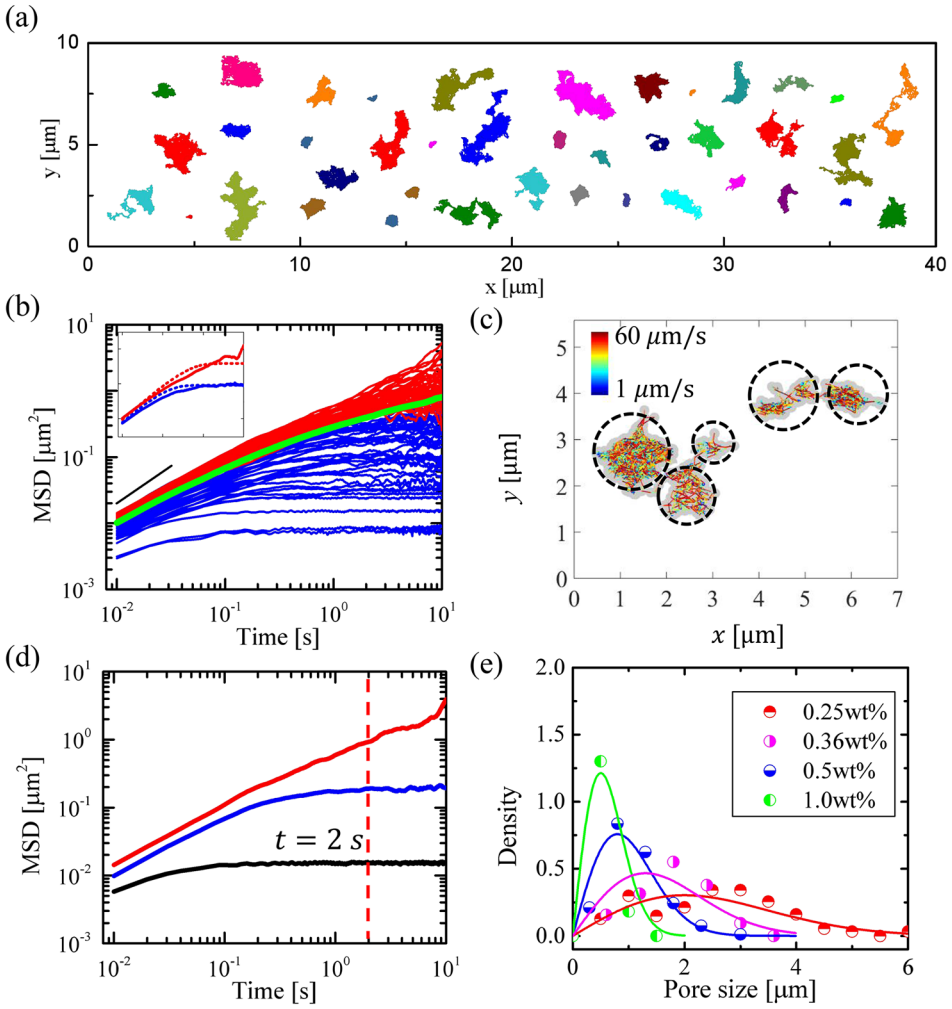

Figure 1. (a) Representative trajectories of NPs in AG hydrogel. NP size d = 500 nm, AG concentration c = 0.36 wt %, and each trajectory lasts longer than 10 s. This map shows that the inherent porous structure in AG gel is highly heterogeneous. (b) Measured time-averaged MSDs (red and blue curves) for 500 nm NPs in 0.36 wt % AG gel. The green curve is the ensemble-averaged MSD. Curves displaying horizontal plateaus at long times are shown in blue, while red indicates the increasing tMSDs at long times. (c) Overlapped trajectories from two 500 nm NPs showing that NPs hop through pathways connecting adjacent pores. The trajectories are color-coded according to the diffusive speed. The gray areas are plotted to estimate the void of the pore by expanding one radius of the NP from the overlapped area of the trajectories. Dashed circles are drawn to show that the pores can be seen as a few spherical pores connected together. (d) Plot showing the choice of t = 2 s as a proper cutoff value for the long-time plateau position of different tMSDs. (e) Pore size distributions in AG gel for different AG concentrations. The distributions obey the Rayleigh distribution (solid curves).

The displacement probability distribution (DPD), another important parameter for NP diffusive dynamics, displays non-Gaussian characteristics (e.g., a sharper peak and narrower waist).[38−40] The tailed DPD, which is more sensitive to heterogeneous spatial structures, is of particular interest for anomalous diffusion. The shape and variation of the tailed DPD have been considered as key features of NP anomalous diffusion in complex media.[38,41,42] As a result, quantitatively characterizing this anomalous diffusion and establishing the connection between the NP dynamics and the surrounding heterogeneous structure are critical to facilitate the efficient use of hydrogels.

In this study, agarose (AG) hydrogels were employed as a model porous medium, and the diffusion of NPs embedded in AG hydrogel was measured using the particle tracking technique. Based on analyses of both the time- and the ensemble-averaged MSD, we developed a method to characterize the nonuniform pore size distribution in hydrogels and unveiled the dynamic and statistical features of the embedded NPs. These diffusive NPs were not completely restricted to individual pores by the adjacent matrix. Instead, they intermittently escaped from single pores through connective channels, manifesting the "hopping" behavior. By clarifying the key mechanisms, including the occurrence of the hopping event, the hydrodynamic effect in a pore, and the pore size distribution, we simulated this scenario using the Monte Carlo (MC) method and quantitatively described all the experimentally observed features.

The representative time-lapse trajectories of 500 nm NPs in 0.36 wt % AG gel are shown in Figure 1a. All the trajectories were tracked for more than 10 s, allowing each NP to adequately probe its ambient space. As the NPs were caged within the hydrogel structures, the void space that these NPs explored outlines the two-dimensional morphology of the pores. This map of trajectories shows that the inherent porous structure in the AG gel is highly heterogeneous with various

https://doi.org/10.1021/acs.jpclett.2c02733
J. Phys. Chem. Lett. 2022, 13, 10612−10620

irregular pore shapes. In addition, partially immobilized NPs were observed because they were stuck in the crowded networks during gel formation. The proportion of these partially immobilized NPs increased with AG concentration and NP size.

The heterogeneous porous structure shown in Figure 1a resulted in diverse dynamic behavior of the embedded NPs. Figure 1b shows the time-averaged MSDs [tMSD or $\overline{r^2(t)}$] of 500 NPs versus lag time t in 0.36 wt % AG hydrogels. The tMSD is mathematically defined as

$$\overline{r^2(t)} = \frac{1}{T-t}\int_0^{T-t} [r(t_0 + t) - r(t_0)]^2 \, dt_0 \quad (1)$$

where T is the duration of the sample trajectory (up to 50 s in this experiment). The ensemble-averaged MSD (eMSD or $\langle r^2(t)\rangle$) is obtained as the statistical mean of all the tMSD data. The eMSD curve in Figure 1b well characterizes the crossover from a linear regime at short times (approximately $t < 0.05$ s) to a subdiffusive regime at long times (approximately $t > 0.1$ s). The slope of unity at short times agrees with the expectation for free diffusion. The slope decreases as time elapses, indicating confined diffusion at long times, i.e., $t > 500$ ms.

In previous studies, only the eMSD results were reported to describe the diffusive behavior in hydrogels or other porous media.[24,25] However, we think that that time-varying tMSDs can be more informative. As each individual tMSD curve reflects the impact of the local structure, all the tMSDs with different slopes can be used to inspect the nonuniformity of the porous structure. Notably, the tMSDs show a wide range of slopes (from 0 to 0.9) at long times, in contrast to the rather uniform slope of unity at short times. This dispersion suggests that the diffusion of the NPs should be affected by complex mechanisms, especially at long times. We propose that the diffusion of the NPs can be explained by the following mechanisms: (1) the pore confinement effect, (2) the hopping of the NP through the pore throat, and (3) the hydrodynamic effect, as discussed more below.

To better understand how pore confinement influences tMSD, we introduce a theoretical model of the confined diffusion of a spherical particle in an immobile spherical pore with a solid wall.[43] The MSD of this confined diffusion can be described as

$$\overline{r^2(t)} = 2nD_m\tau(1 - e^{-t/\tau}) \quad (2)$$

where $D_m = k_BT/3\pi\mu d$ is the microscopic diffusivity of the unconfined NP (μ is the viscosity of the fluid); $\tau = R^2/5D_m$ is the typical residence time of the NP in the pore with radius R; and $n = 1, 2, 3$ is the dimensionality of the diffusive process. The wall of the pore is assumed to be reflecting since wall adsorption is largely avoided by adding surfactant. In this simple case of an NP confined in a spherical pore, the tMSD based on eq 2 manifests three-stage behavior. At short times ($t \ll \tau$), the tMSD curve is linear, indicating a diffusive stage where the wall effect is negligible. As time increases to $t \sim \tau$, the tMSD curve becomes subdiffusive due to the wall−particle interaction. At long times ($t \gg \tau$), the MSD curve becomes a horizontal plateau close to $6R^2/5$. Approximately 44% of the measured tMSDs (displayed in blue in Figure 1b) can be well described by eq 2. The blue curve and its fit (dashed curve) in the inset of Figure 1b demonstrate this good agreement.

One can easily observe that some of the tMSD curves clearly keep rising at long times (red curves in Figure 1b), which deviates from the theoretical prediction of ideal confined diffusion. We speculate that this deviation (i.e., the longer displacement of the NP) is caused by the hopping of the NP through the pore throat. Figure 1c shows the overlapped trajectories (lasting for 60 s) from some NPs, which clearly show the NP hopping through the narrow pathway between adjacent pores. From the trajectories, we can distinguish a pore from a pathway by the residence time of a NP (the NP's residence time is much longer in a pore than in a pathway). Based on 20 different overlapped trajectories that manifest the connecting narrow pathways, we estimate the normalized pathway width to be $W/2R = 0.44 \pm 0.20$. More interestingly, NP hopping is not a rare event. As shown in Figure 1b, the rising tMSDs (displayed in red) at long times occupy more than 50% of all the tMSD curves; this not only reflects the spatial heterogeneity of the pore structure in hydrogels, it also allows us to evaluate the occurrence of hopping events.

The next question is how to quantitatively describe the pore size distribution and the hopping probability. The multistage theoretical MSD can help distinguish dominant mechanisms at different time scales. In particular, the plateau of the theoretical MSD approaches $6R^2/5$ at long times, which reflects the geometric confinement of local pores. By defining the proper cutoff value for each tMSD as $t = 2$ s, as marked by the dashed line in Figure 1d, we can determine the plateau value $6R^2/5$ of every single tMSD curve and obtain the pore size R. This selection of the cutoff value is based on the fact that most tMSDs have just entered the plateau stage at this moment. Even for those tMSDs that keep rising at long times, the increases are relatively small beyond $t = 2$ s; thus, this selection should avoid the overestimation of pore size R.

The pore size distribution was established by measuring the pore size over 100 individual tMSD curves. Figure 1e shows the pore size distributions in AG gel at different AG concentrations. The pore size distribution is rather broad, in agreement with a recent experiment.[44] We notice that the diffusion of NPs that are located in large connecting pores has an important contribution on the increase of the eMSD at long times. The pore size distribution in our experiment obeys the Rayleigh distribution rather than the Gaussian distribution,[24,45] as shown by the fit curve in Figure 1e. This can be explained by modeling the pores of the hydrogel system as spaces in a random network of straight fibers.[46] The probability density function of the Rayleigh distribution is described by $p(R) = \frac{R}{C^2}\exp\left(-\frac{R^2}{2C^2}\right)$, where the parameter C also indicates the most probable pore radius R_p (i.e., $R_p = C$). Table 1 lists the most probable pore radius R_p and the mean pore radius R_m. We also compare our pore size data with previous experimental results (see Figure S1 in the Supporting Information), and we find that the most probable pore radius R_p is consistent very well with previous results obtained by fluorescence recovery after photobleaching (FRAP) and AFM.[45,47] Although our data are slightly larger than the microscopy results[24] in Figure S1b, the variation tendencies are quite similar. Both R_p and R_m decrease with increasing AG concentration, suggesting a power law dependence of R_p or R_m on the AG concentration c. We fit the data by $R_p \sim c^{-\gamma}$ with $\gamma \approx 0.9$, which is close to the value predicted by De Gennes for a network of flexible chains (0.75).[48] The Rayleigh distribution exhibits a heavier tail on the side of the larger radius compared to the side of the smaller radius. Note that modeling the pore size using a Gaussian distribution cannot depict this asymmetric distribution.

https://doi.org/10.1021/acs.jpclett.2c02733
J. Phys. Chem. Lett. 2022, 13, 10612−10620

Table 1. Pore Size Distribution and Probability of NPs Being Trapped in a Pore

	Most probable radius R_p	Mean radius R_m	Probability of being trapped (EXP)	Probability of being trapped (MC)
d = 500 nm, c = 0.25%	1020 nm	1318 nm	27%	33.5%
d = 500 nm, c = 0.36%	758 nm	877 nm	44%	50.6%
d = 500 nm, c = 0.50%	485 nm	589 nm	73%	78.3%
d = 500 nm, c = 1.0%	262 nm	306 nm	100%	99.7%
d = 200 nm, c = 1.0%	262 nm	306 nm	47%	48.2%
d = 100 nm, c = 1.0%	262 nm	306 nm	0%	1.4%

Knowing the pore size distribution, we developed a numerical approach based on the MC method to describe the diffusive dynamics of NPs in hydrogels. We used the time step Δt = 1 ms to generate NP movements $L = \sqrt{2nD_s\Delta t}$. One key issue here is the hydrodynamic correction of the drag coefficient of the diffusivity D_s due to the wall effect. Based on Brenner's theory about the drag force of a particle moving toward a wall,[49,50] the diffusivity in the simulation can be expressed as $D_s = k_BT/3\pi\mu d\xi$, where $\xi = (6h^2 + 9Rh + 2R^2)/(6h^2 + 2Rh)$ is the correction factor and h is the distance from the NP's center to the wall. This theoretical model has been verified in our previous experiments on NP diffusion near a solid wall.[51] It is necessary to indicate that there is another hydrodynamic model,[52] which solves the NP's mobility by assuming that a spherical particle of radius R moves in a fluid-filled spherical pore. However, in our experiments we found that this model largely overestimates the hydrodynamic drag force in the pore, because the fluid flow through the hydrogel networks is not taken into account. Our treatment using Brenner's theory is in line with Ogston's model,[46,53,54] in which the network is considered to be formed by long straight fibers. When the hydrogel concentration is not high and the NP's size is relatively small, Brenner's theory might be a more appropriate approximation.[50,51] Note that the time step should be short enough to match the time interval between two successive frames of the experimental video. The detailed description of the MC simulation is provided in the Supporting Information.

Figure 2 compares the simulated (MC) and experimental MSD curves for 500 nm NPs in 0.36 wt % AG gel. Our MC simulation reproduces the experimental features of both the tMSDs and the eMSDs by considering the hopping events and wall hydrodynamic effects Figure 2a. We first assumed a reflecting wall for all the pores in the MC simulation. Despite the similar behavior of the tMSD curves at short times, all the tMSD curves of the MC simulations do not rise; rather, they maintain a horizontal plateau at long times, which is distinct from the experimental results in Figure 2b. The deviation becomes clearer if one examines the gap between the MC and the experimental eMSD curves at long times in Figure 2b. This deviation can only be explained by the hopping of some NPs from the original pore through the pathway to another pore, as shown in Figure 1c.

To demonstrate this phenomenon, we introduced a hopping probability p_h in the MC simulation. Each time an NP reached the wall of the pore, the MC program randomly generated a value p $(0 \le p \le 1)$. If $p \le p_h$, the NP hopped to an adjacent pore; otherwise, it rebounded from the wall. By setting an average value p_h = 0.007 for the case of 500 nm NPs in 0.36 wt % AG gel, we reproduce tMSDs similar to the experimental values in Figure 2a. The eMSD obtained by MC simulation also overlaps with the experimental eMSD. This agreement demonstrates that our model indeed reflects the dominant mechanisms of NP diffusion in a complex hydrogel. For other cases, based on the fact that observed hopping events through connecting pathways increase as the pore radius increases and the NP size decreases, we propose the following exponential relation to describe the hopping probability p_h of each step in the MC simulation: $p_h = \exp(-14a/R_p)$. Furthermore, if the wall hydrodynamic effect is ignored, the MSDs obtained by MC simulation are always larger than the experimental MSDs due to the underestimation of the drag force on the diffusive NP near the wall, as shown in Figure 2c. This indicates that the hydrodynamic effect should be considered in the proposed model.

Based on the MC method, we reproduced all the MSDs at various AG concentrations using different NPs. As shown in Figure 3, all the MC results (the second row) predict the experimental results (the first row) very well. A comparison between Figure 3a–c and Figure 3f–h demonstrates the influence of the AG concentration or, in other words, the influence of the pore size. Increasing the AG concentration significantly reduces the most probable pore size and the pore size variance, resulting in smaller pore sizes and less dispersion in the tMSDs. The hopping possibility is almost completely eliminated when the AG concentration reaches 1%, which corresponds to a pore size of approximately $2R_p$ = 520 nm,

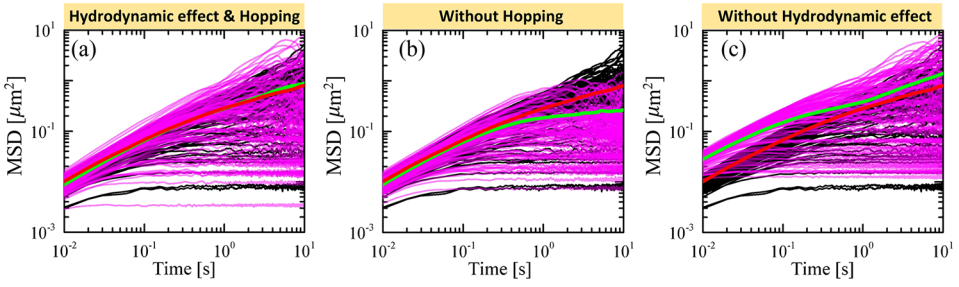

Figure 2. Experimental (black curves) and MC (purple curves) MSD curves for 500 nm NPs in 0.36 wt % AG gel. The red lines represent the experimental eMSD, and the green lines represent the numerical eMSD. (a) The MC simulation taking hopping and hydrodynamic effects into account shows good agreement with experiment. (b) The MC simulation does not reproduce the long-time rising MSDs if NP hopping is not included. (c) The simulation produces larger MSDs if the wall hydrodynamic effect is absent.

https://doi.org/10.1021/acs.jpclett.2c02733
J. Phys. Chem. Lett. 2022, 13, 10612−10620

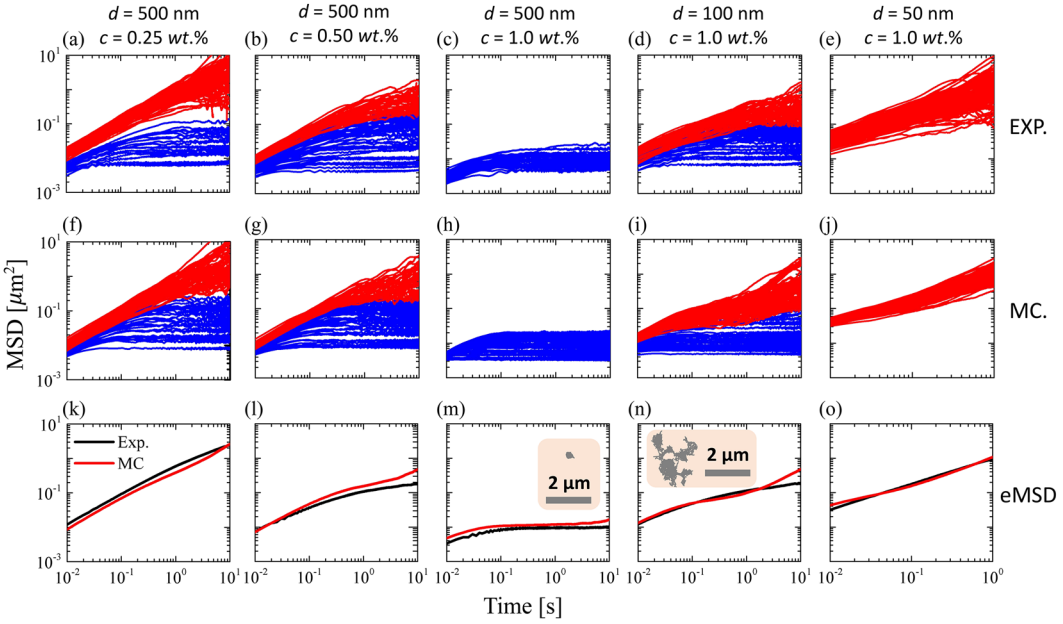

Figure 3. Comparison of the tMSDs obtained from experiments (first row) and MC simulations (second row) for five different cases. The third row shows the good agreement between the experimental (black) and simulated (red) eMSDs. The tMSDs that manifest plateaus at long times are shown in blue, while those manifesting increase tendencies at long times are shown in red. The insets show the typical trajectories at the corresponding conditions.

similar to the NP diameter. The diameter of the pathway connecting nearby pores also decreases with the pore size and AG concentration; thus, all the tMSDs exhibit horizontal plateaus, Figure 3c,h. The influence of the NP size is shown in Figure 3c–e and Figure 3h–j, where the pore size of the hydrogel is fixed. Decreasing the NP radius significantly enhances the NP mobility and likelihood of hopping. When the NP diameter decreases to 100 nm, all the NPs in the experiments exhibit hopping behavior and show rising tMSDs rather than horizontal plateaus at long times. In particular, the eMSD of the 50 nm NP shows a linear dependence with time (eMSD $\sim t$), indicating a surprising diffusive behavior from the statistics. We notice that similar results have been reported,[55] in which the confinement ratio CR (defined as NP diameter/pore size) was proposed to illustrate the confinement from hydrogel networks. From Figure 3c,m, we observe that strong confinement effect slows the NP's diffusion when CR = 0.82. On the contrary, from Figure 3e,o, the confinement is much weaker when CR = 0.08.

The good agreement in Figure 3 indicates that the equation $p_h = \exp(-14a/R_p)$ can describe the hopping probability over a wide range of NP and pore sizes. By considering the hopping mechanism, our MC simulation also provides a way to quantitatively estimate the size selectivity of hydrogels by calculating the probability that a NP is always trapped in the same pore. The last two columns of Table 1 provide the probabilities that the NPs do not hop out of their original pores, corresponding to the ratio of blue tMSD curves to red tMSD curves in different cases. The MC simulations give trapping probabilities consistent with the experiments. The results also suggest size-dependent transport behavior. In the 1.0% AG gel, the transport of 500 nm NPs is fully constrained to the local pores, whereas the 100 nm NPs diffuse over much longer distances through the connecting pathways, as demonstrated in the insets of Figure 3m,n. Although the MC simulation has reproduced well the statistical features from the experiments, we would like to underscore that the MC method is subject to the limitation in modeling the hydrodynamic interactions. According to the work from Hansing and Netz,[56] the hydrodynamic interactions between a NP and the hydrogel polymers can be calculated by summing the far-field hydrodynamic force and the lubrication forces, which shows strong inhomogeneous hydrodynamic screening effect and good agreement with experiments.

In addition to the MSD characteristics analyzed above, the DPD is necessary for understanding anomalous diffusion in porous media. The shape and time variation of the DPD were recently found to be crucial properties of anomalous diffusion.[37,38,41,42] We calculated the ensemble-averaged DPD from experiment and MC simulation. To compare the results, the standard Gaussian distribution with probability density function $G_s = \frac{1}{\sqrt{2\pi}} \exp(-(\Delta x/\sigma)^2/2)$ is introduced, where σ is the standard deviation of displacement.

Representative G_s results from experiments are shown in Figure 4a,c for 500 and 200 nm NPs, respectively. The measured DPDs exhibit lambda (Λ) shapes with a central peak and two extended tails deviating from the standard Gaussian distribution. When $|\Delta x/\sigma| > 2$, the tailed distribution is exponential, following $G_s \sim \exp(\pm k\Delta x/\sigma)$, where k demonstrates the slope in the logarithmic Figure 4. This exponential tendency has received considerable attention related to diffusing diffusivity in anomalous diffusion,[34,37,38] and we think that the diffusing behavior reflects the pore size dispersion in hydrogels. Such non-Gaussian behavior of the DPD can be understood as the averaging over different NPs in different confinements that leads to different Gaussian widths, which has been observed in systems with various confinements.[57]

The heavier tails of the DPD compared to the standard Gaussian distribution are attributed to the higher likelihood of the NPs hopping through the pathway. Thus, the slope of the

https://doi.org/10.1021/acs.jpclett.2c02733
J. Phys. Chem. Lett. 2022, 13, 10612−10620

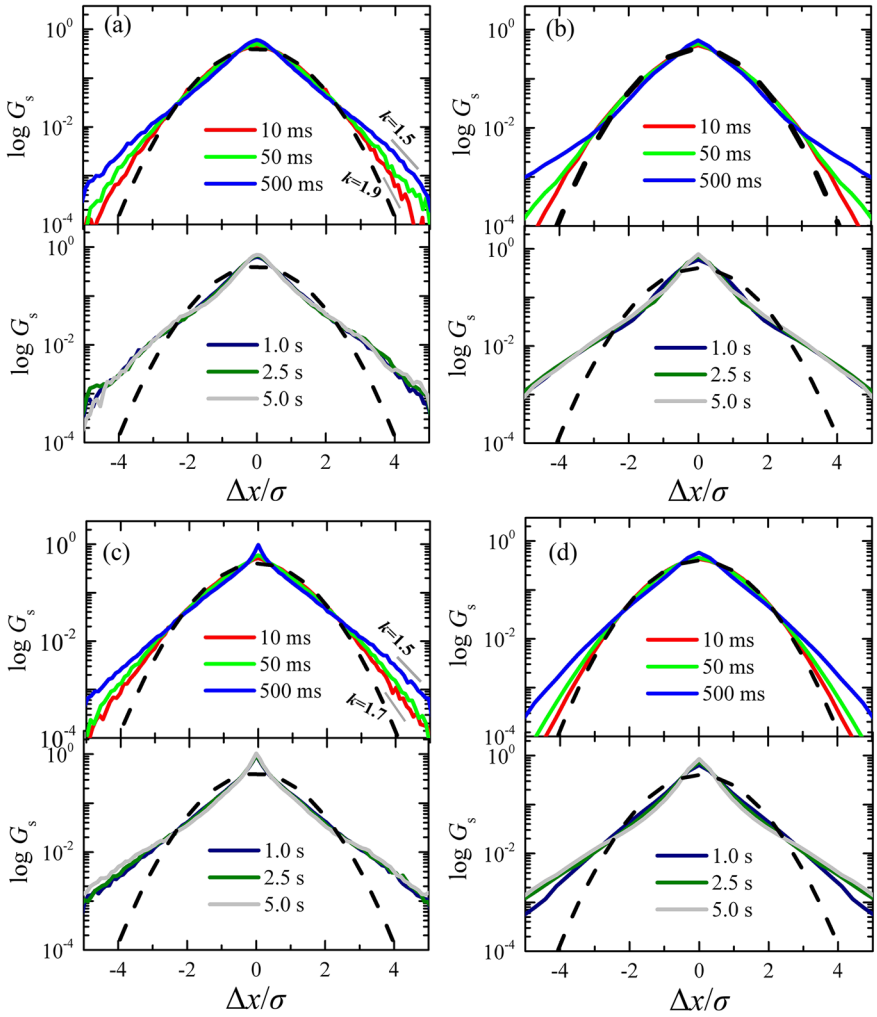

Figure 4. DPDs plotted logarithmically against normalized displacement. (a) The experimental result for 500 nm NPs in 0.5% AG gel and (c) the experimental result for 200 nm NPs in 1% AG gel. (b) and (d) are the MC results corresponding to (a) and (c), respectively. σ is the standard deviation of displacement and was used to normalize the displacement.

exponential tail provides a statistical indicator of the void connectivity of the porous hydrogel structure. This non-Gaussian feature emerges over the full range of our experimental time scales from milliseconds to seconds. The full-time non-Gaussian G_s differs from the results obtained in softer confinements like polymer solutions, in which the non-Gaussian behavior only exists on intermediate time scales.[30,31,58] More intriguingly, the non-Gaussian behavior exhibits a two-staged time dependence. That is, at short times ($t \leq 500$ ms), the tail part becomes heavier as time increases (the slope parameter k decreases from approximately 1.8 to 1.5 in Figure 4a,c), while the DPD remains unchanged as time further elapses ($t > 1$ s). The critical time here corresponds to the transition time in the eMSD curve under the same condition (Figure 3).

It is noteworthy that the probability density function of the exponential tails can be rewritten as $G_s \sim \exp(\pm\Delta x/\lambda(t))$, where $\lambda(t)$ is the characteristic length of the tail distribution (and also represents the typical length of the confinement from the hydrogel networks at a time t). Lee et al. have successfully used this equation to characterize the hydrogel networks.[37] Based on this equation, we fit the exponential tails of the DPDs at different times and plot the data of λ *vst* for 500 nm NPs in three different AG concentrations (Figure 5). Figure 5 demonstrates that the values of λ are smaller at higher AG concentrations as the NP will experience stronger confinements. For the same AG concentration, we observe a transition from a short-time regime (approximately $t < 0.1$ s) showing a power-law dependence of $\lambda \sim t^{0.5}$ to a long-time regime. The short-time behavior is consistent with the result from Wang et

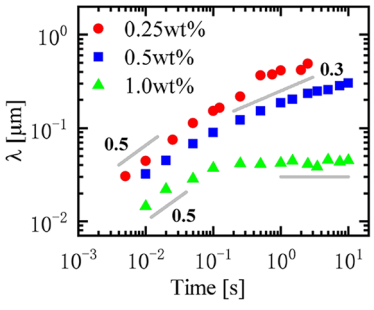

Figure 5. Temporal variation of the characteristic length of the exponential tail $\lambda(t)$ using 500 nm NPs, revealing a transition from a short-time regime with $\lambda \sim t^{0.5}$ to a long-time regime with a much slower increase of λ.

https://doi.org/10.1021/acs.jpclett.2c02733
J. Phys. Chem. Lett. 2022, 13, 10612−10620

al.[59] However, the long-time behavior becomes more complex. For low AG concentration (0.25−0.5 wt %), a power-law relation close to $\lambda \sim t^{0.3}$ is found, similar to the relation $\lambda \sim t^{0.33}$ reported in ref 37; for high AG concentration (1.0 wt %), a plateau at about $\lambda \sim 45$ nm is obtained, reflecting that no hopping can occur in such a high concentration when 500 nm NPs are used (see Figure 3c).

Our MC simulations reproduced the lambda shape and time variation of the DPDs, as shown in Figure 4b,d. This agreement demonstrates that our method can reproduce the main dynamic and statistical features of anomalous confined diffusion in porous hydrogels by accounting for the three dominant mechanisms: confined NP diffusion, hopping behavior through void connective pathways, and the hydrodynamic effect. We notice that, at very short times ($t < 50$ ms in Figure 4), the DPDs in the range $-2.5\sigma < x < 2.5\sigma$ are approximately Gaussian, reflecting the fact that most DPDs calculated from individual NPs are still Gaussian when $t \sim 10$ ms. The seemingly straight tails of the lambda shapes in the semilogarithmic plots are similar for different cases when $t \geq 5$ s, suggesting a universal exponential distribution for the two tails: $G_s \sim \exp(\pm 1.45\Delta x/\sigma)$. In total, our hybrid model that considers the above mechanisms can fully describe the transport dynamics of NPs in porous media and is thus helpful for the design of biomedical porous materials.

On top of the mechanisms like hopping and hydrodynamic effect analyzed above, it is noteworthy to mention that other factors could also influence particle diffusion in hydrogels. For instance, Wolde-Kidan et al. recently used fluorescence microscopy to measure the concentration profile of dextran molecules in hydrogels,[44] and they concluded that the macromolecule penetration into hydrogels for steric particle−hydrogel interactions is governed by an elastic size-filtering mechanism. Different from spherical NPs, for flexible macromolecules and polymer chains the entropy effect might also play an important role.[54,60]

In summary, we studied the diffusive motion of NPs in hydrogels to clarify the mechanisms of confined diffusion and the characteristics of NP dynamics in porous media. The NP diffusive motion was measured using particle tracking experiments, and both the time- and ensemble-averaged MSDs were examined. We not only developed a robust method to estimate the heterogeneous pore size distribution and void connectivity in the hydrogel, we also revealed the anomalous diffusion dynamics of the embedded NPs. We found that diffusive NPs can intermittently hop between single pores through void connective pathways, thereby exploring more space in adjacent pores. We then simulated this scenario using the MC method and confirmed the importance of hopping events in porous diffusion. The anomalous diffusion of confined NPs can be well illustrated by combining the hopping mechanism and the hydrodynamic near-wall effect. Our results provide a hybrid model to predict the dynamics of NPs in hydrogels and other porous media. This model can provide valuable information and an analytical method for controlled delivery and selective transport in various porous media.

■ ASSOCIATED CONTENT

Supporting Information

The Supporting Information is available free of charge at https://pubs.acs.org/doi/10.1021/acs.jpclett.2c02733.

Experimental materials and methods including reagent, sample preparation, and particle tracking experiment; pore size characterization by X-ray diffraction and a comparison with previous measurements; Monte Carlo simulation including the main ideal of MC simulation, pore size generation, NP−wall interaction, hydrodynamic effect, and main procedure of MC simulation; and Figures S1−S3 (PDF)

■ AUTHOR INFORMATION

Corresponding Authors

Guoqing Hu − *Department of Engineering Mechanics, Zhejiang University, Hangzhou 310027, China;* orcid.org/0000-0001-9451-5336; Email: ghu@zju.edu.cn

Xu Zheng − *State Key Laboratory of Nonlinear Mechanics, Beijing Key Laboratory of Engineered Construction and Mechanobiology, Institute of Mechanics, Chinese Academy of Sciences, Beijing 100190, China;* orcid.org/0000-0002-2398-9283; Email: zhengxu@lnm.imech.ac.cn

Authors

Chundong Xue − *State Key Laboratory of Nonlinear Mechanics, Beijing Key Laboratory of Engineered Construction and Mechanobiology, Institute of Mechanics, Chinese Academy of Sciences, Beijing 100190, China; School of Optoelectronic Engineering and Instrumentation Science, Dalian University of Technology, Dalian 116024, China;* orcid.org/0000-0002-5259-4491

Yirong Huang − *State Key Laboratory of Nonlinear Mechanics, Beijing Key Laboratory of Engineered Construction and Mechanobiology, Institute of Mechanics, Chinese Academy of Sciences, Beijing 100190, China*

Complete contact information is available at: https://pubs.acs.org/10.1021/acs.jpclett.2c02733

Notes

The authors declare no competing financial interest.

■ ACKNOWLEDGMENTS

The authors acknowledge the National Natural Science Foundation of China (Grant Nos. 11832017, 12172081, and 12072350), the Natural Science Foundation of Liaoning Province (Nos. 2021-MS-133), and the China Postdoctoral Science Foundation (2019M651106).

■ REFERENCES

(1) Li, J.; Mooney, D. Designing Hydrogels for Controlled Drug Delivery. *Nat. Rev. Mater.* **2016**, *1*, 16071.

(2) Ceylan, H.; Yasa, I.; Yasa, O.; Tabak, A. F.; Giltinan, J.; Sitti, M. 3D-Printed Biodegradable Microswimmer for Theranostic Cargo Delivery and Release. *ACS Nano* **2019**, *13*, 3353−3362.

(3) Tibbitt, M. W.; Dahlman, J. E.; Langer, R. Emerging Frontiers in Drug Delivery. *J. Am. Chem. Soc.* **2016**, *138*, 704−717.

(4) Zhang, Y.; Khademhosseini, A. Advances in Engineering Hydrogels. *Science* **2017**, *356*, No. eaaf3627.

(5) Skilling, K. J.; Citossi, F.; Bradshaw, T. D.; Ashford, M.; Kellam, B.; Marlow, M. Insights into Low Molecular Mass Organic Gelators: A Focus on Drug Delivery and Tissue Engineering Applications. *Soft Matter* **2014**, *10*, 237−256.

(6) Seliktar, D. Designing Cell-Compatible Hydrogels for Biomedical Applications. *Science* **2012**, *336*, 1124−1128.

(7) Lee, S.; Sasaki, D.; Kim, D.; Mori, M.; Yokota, T.; Lee, H.; Park, S.; Fukuda, K.; Sekino, M.; Matsuura, K.; Shimizu, T.; Someya, T.

Ultrasoft Electronics to Monitor Dynamically Pulsing Cardiomyocytes. *Nat. Nanotechnol.* **2019**, *14*, 156−160.
(8) Yuk, H.l.; Lu, B.; Zhao, X. Hydrogel Bioelectronics. *Chem. Soc. Rev.* **2019**, *48*, 1642−1667.
(9) Peppas, N. A.; Van Blarcom, D. S. Hydrogel-based Biosensors and Sensing Devices for Drug Delivery. *J. Controlled Release* **2016**, *240*, 142−150.
(10) Grainger, D. W. Wound Healing Enzymatically crosslinked scaffolds. *Nat. Mater.* **2015**, *14*, 662−664.
(11) Cai, F.; Wang, J. X.; Qian, X.; et al. Extremely Stretchable Strain Sensors Based on Conductive Self-Healing Dynamic Cross-Links Hydrogels for Human-Motion Detection. *Adv. Sci.* **2017**, *4*, 1600190.
(12) El-Sherbiny, I.; Khalil, I.; Ali, I.; Yacoub, M. Updates on Smart Polymeric Carrier Systems for Protein Delivery. *Drug Dev. Ind. Pharm.* **2017**, *43*, 1567−1583.
(13) Vashist, A.; Kaushik, A.; Vashist, A.; Sagar, V.; Ghosal, A.; Gupta, Y. K.; Ahmad, S.; Nair, M. Advances in Carbon Nanotubes-Hydrogel Hybrids in Nanomedicine for Therapeutics. *Adv. Healthcare Mater.* **2018**, *7*, 1701213.
(14) Parker, J.; Mitrousis, N.; Shoichet, M. S. Hydrogel for Simultaneous Tunable Growth Factor Delivery and Enhanced Viability of Encapsulated Cells in Vitro. *Biomacromolecules* **2016**, *17* (2), 476−484.
(15) Lin, C.; Metters, A. T. Hydrogels in Controlled Release Formulations: Network Design and Mathematical Modeling. *Adv. Drug Delivery Rev.* **2006**, *58*, 1379−1408.
(16) Wu, Y.; Wang, K.; Huang, S.; Yang, C.; Wang, M. Near-Infrared Light-Responsive Semiconductor Polymer Composite Hydrogels: Spatial/Temporal-Controlled Release via a Photothermal "Sponge" Effect. *ACS Appl. Mater. Interfaces* **2017**, *9*, 13602−13610.
(17) Wang, K.; Betancourt, T.; Hall, C. Computational Study of DNA-Cross-Linked Hydrogel Formation for Drug Delivery Applications. *Macromolecules* **2018**, *51*, 9758−9768.
(18) Sepantafar, M.; Maheronnaghsh, R.; Mohammadi, H.; Radmanesh, F.; Hasani-Sadrabadi, M. M.; Ebrahimi, M.; Baharvand, H. Engineered Hydrogels in Cancer Therapy and Diagnosis. *Trends Biothechnol.* **2017**, *35*, 1074−1087.
(19) Um, E.; Oh, J.; Granick, S.; Cho, Y.-K. Cell Migration in Microengineered Tumor Environments. *Lab Chip* **2017**, *17*, 4171−4185.
(20) Cai, Y.; Schwartz, D. Mapping the Functional Tortuosity and Spatiotemporal Heterogeneity of Porous Polymer Membranes with Super-Resolution Nanoparticle Tracking. *ACS Appl. Mater. Interfaces* **2017**, *9*, 43258−43266.
(21) Edery, Y.; Guadagnini, A.; Scher, H.; Berkowitz, B. Origins of anomalous transport in heterogeneous media: Structural and dynamic controls. *Water Resour. Res.* **2014**, *50*, 1490−1505.
(22) Dai, Q.; Wilhelm, S.; Ding, D.; Syed, M. A.; Sindhwani, S.; Zhang, Y.; Chen, Y. Y.; MacMillan, P.; Chan, W. C. Quantifying the Ligand-Coated Nanoparticle Delivery to Cancer Cells in Solid Tumors. *ACS Nano* **2018**, *12*, 8423−8435.
(23) Yu, M.; Xu, L.; Tian, F.; Su, Q.; Zheng, N.; Yang, Y.; Wang, J.; Wang, A.; Zhu, C.; Guo, S.; Zhang, X.; Gan, Y.; Shi, X.; Gao, H. Rapid Transport of Deformation-Tuned Nanoparticles across Biological Hydrogels and Cellular Barriers. *Nat. Commun.* **2018**, *9*, 2607.
(24) Jiang, L.; Granick, S. Real-Space, in Situ Maps of Hydrogel Pores. *ACS Nano* **2017**, *11*, 204−212.
(25) Yu, M.; Song, W.; Tian, F.; Dai, Z.; Zhu, Q.; Ahmad, E.; Guo, S.; Zhu, C.; Zhong, H.; Yuan, Y.; Zhang, T.; Yi, X.; Shi, X.; Gan, Y.; Gao, H. Temperature- and Rigidity-mediated Rapid Transport of Lipid Nanovesicles in Hydrogels. *Proc. Nat. Acad. Sci. U. S.* **2019**, *116*, 5362−5369.
(26) Wang, D.; Wu, H.; Liu, L.; Chen, J.; Schwartz, D. K. Diffusive Escape of a Nanoparticle from a Porous Cavity. *Phys. Rev. Lett.* **2019**, *123*, 118002.
(27) Skaug, M. J.; Wang, L.; Ding, Y.; Schwartz, D. K. Hindered Nanoparticle Diffusion and Void Accessibility in A Three-dimensional Porous Medium. *ACS Nano* **2015**, *9*, 2148−2156.
(28) Richter, S.; Matzker, R.; Schroter, K. Gelation Studies, 4. Why do "Classical" Methods like Oscillatory Shear Rheology and Dynamic Light Scattering for Characterization of the Gelation Threshold Sometimes Not Provide Identical Results Especially on Thermoreversible Gels? *Macromol. Rapid Commun.* **2005**, *26*, 1626−1632.
(29) Estroff, L. A.; Leiserowitz, L.; Addadi, L.; Weiner, S.; Hamilton, A. D. Characterization of an Organic Hydrogel: A Cryo-Transmission Electron Microscopy and X-ray Diffraction Study. *Adv. Mater.* **2003**, *15*, 38−42.
(30) Wang, B.; Kuo, J.; Bae, S. C.; Granick, S. When Brownian Diffusion Is Not Gaussian. *Nat. Mater.* **2012**, *11*, 481−485.
(31) Xue, C.; Zheng, X.; Chen, K.; Tian, Y.; Hu, G. Probing Non-Gaussianity in Confined Diffusion of Nanoparticles. *J. Phys. Chem. Lett.* **2016**, *7*, 514−519.
(32) Chechkin, A. V.; Seno, F.; Metzler, R.; Sokolov, I. M. Brownian yet Non-Gaussian Diffusion: From Superstatistics to Subordination of Diffusing Diffusivities. *Phys. Rev. X.* **2017**, *7*, 021002.
(33) Phillies, G. D. J. In Complex Fluids the Gaussian Diffusion Approximation Is Generally Invalid. *Soft Matter* **2015**, *11*, 580−586.
(34) Xu, Z.; Dai, X.; Bu, X.; Yang, Y.; Zhang, X.; Man, X.; Zhang, X.; Doi, M.; Yan, L. Enhanced Heterogeneous Diffusion of Nanoparticles in Semiflexible Networks. *ACS Nano* **2021**, *15*, 4608−4616.
(35) Dai, X.; Zhang, X.; Gao, L.; Xu, Z.; Yan, L. Topology Mediates Transport of Nanoparticles in Macromolecular Networks. *Nat. Commun.* **2022**, *13*, 4094.
(36) Hofling, F.; Franosch, T. Anomalous transport in the crowded world of biological cells. *Rep. Prog. Phys.* **2013**, *76*, 046602.
(37) Lee, C. H.; Crosby, A. J.; Emrick, T.; Hayward, R. C. Characterization of Heterogeneous Polyacrylamide Hydrogels by Tracking of Single Quantum Dots. *Macromolecules* **2014**, *47*, 741−749.
(38) Chubynsky, M. V.; Slater, G. W. Diffusing Diffusivity: A Model for Anomalous, yet Brownian, Diffusion. *Phys. Rev. Lett.* **2014**, *113*, 098302.
(39) He, W.; Song, H.; Su, Y.; Geng, L.; Ackerson, B. J.; Peng, H. B.; Tong, P. Dynamic Heterogeneity and Non-Gaussian Statistics for Acetylcholine Receptors on Live Cell Membrane. *Nat. Commun.* **2016**, *7*, 11701.
(40) Lanoiselee, Y.; Moutal, N.; Grebenkov, D. S. Diffusion-limited Reactions in Dynamic Heterogeneous Media. *Nat. Commun.* **2018**, *9*, 4398.
(41) Cherstvy, A.; Thapa, S.; Wagner, C. E.; Metzler, R. Non-Gaussian, Non-ergodic, and Non-Fickian Diffusion of Tracers in Mucin Hydrogels. *Soft Matter* **2019**, *15*, 2526−2551.
(42) Krapf, D.; Lukat, N.; Marinari, E.; Metzler, R.; Oshanin, G.; Selhuber-Unkel, C.; Squarcini, A.; Stadler, L.; Weiss, M.; Xu, X. Spectral Content of a Single Non-Brownian Trajectory. *Phys. Rev. X.* **2019**, *9*, 011019.
(43) Ochab-Marcinek, A.; Hołyst, R. Scale-Dependent Diffusion of Spheres in Solutions of Flexible and Rigid Polymers: Mean Square Displacement and Autocorrelation Function for FCS and DLS Measurements. *Soft Matter* **2011**, *7*, 7366−7374.
(44) Wolde-Kidan, A.; Herrmann, A.; Prause, A.; Gradzielski, M.; Haag, R.; Block, S.; Netz, R. R. Particle Diffusivity and Free-Energy Profiles in Hydrogels from Time-Resolved Penetration Data. *Biophys. J.* **2021**, *120*, 463.
(45) Maaloum, M.; Pernodet, N.; Tinland, B. Agarose Gel Structure using Atomic Force Microscopy: Gel Concentration and Ion Strength Effects. *Electrophoresis* **1997**, *18*, 55−58.
(46) Ogston, A. G. The Spaces in A Uniform Random Suspension of Fibres. *Trans. Faraday Soc.* **1958**, *54*, 1754−1757.
(47) Tinland, B.; Pernodet, N.; Weill, G. Field and Pore Size Dependence of the Electrophoretic Mobility of DNA: a Combination of Fluorescence Recovery after Photobleaching and Electric Birefringence Measurements. *Electrophoresis* **1996**, *17*, 1046−1051.
(48) de Gennes, P. G.*Scaling Concepts in Polymer Physics*; Cornell University Press: Ithaca, NY, 1979.
(49) Brenner, H. The Slow Motion of A Sphere through A Viscous Fluid towards A Plane Surface. Chem. *Eng. Sci.* **1961**, *16*, 242−251.

https://doi.org/10.1021/acs.jpclett.2c02733
J. Phys. Chem. Lett. 2022, 13, 10612−10620

(50) Banerjee, A.; Kihm, K. Experimental Verification of Near-wall Hindered Diffusion for The Brownian Motion of Nanoparticles using Evanescent Wave Microscopy. *Phys. Rev. E* **2005**, *72*, 042101.
(51) Zheng, X.; Shi, F.; Silber-Li, Z. Study on The Statistical Intensity Distribution (SID) of Fluorescent Nanoparticles in TIRFM Measurement. *Microfluid. Nanofluid.* **2018**, *22*, 127.
(52) Valentine, M. T.; Kaplan, P. D.; Thota, P. D.; Crocker, J. C.; Gisler, T.; Prud'homme, R. K.; Beck, M.; Weitz, D. A. Investigating the Microenvironments of Inhomogeneous Soft Materials with Multiple Particle Tracking. *Phys. Rev. E* **2001**, *64*, 061506.
(53) Ogston, A. G.; Preston, B. N.; Wells, J. D. On the Transport of Compact Particles through Solutions of Chain-Polymers. *Proc. R. Soc. London A* **1973**, *333*, 297−316.
(54) Jia, D.; Muthukumar, M. Electrostatically Driven Topological Freezing of Polymer Diffusion at Intermediate Confinements. *Phys. Rev. Lett.* **2021**, *126*, 057802.
(55) Parrish, E.; Caporizzo, M. A.; Composto, R. J. Network Confinement and Heterogeneity Slows Nanoparticle Diffusion in Polymer Gels. *J. Chem. Phys.* **2017**, *146*, 203318.
(56) Hansing, J.; Netz, R. R. Hydrodynamic Effects on Particle Diffusion in Polymeric Hydrogels with Steric and Electrostatic Particle-Gel Interactions. *Macromolecules* **2018**, *51*, 7608−7620.
(57) Mitterwallner, B. G.; Schreiber, C.; Daldrop, J. O.; Rädler, J. O.; Netz, R. R. Non-Markovian Data-Driven Modeling of Single-Cell Motility. *Phys. Rev. E* **2020**, *101*, 032408.
(58) Xue, C.; Shi, X.; Tian, Y.; Zheng, X.; Hu, G. Diffusion of Nanoparticles with Activated Hopping in Crowded Polymer Solutions. *Nano Lett.* **2020**, *20*, 3895−3904.
(59) Wang, B.; Anthony, S. M.; Bae, S. C.; Granick, S. Anomalous yet Brownian. *Proc. Nat. Acad. Sci. U. S.* **2009**, *106*, 15160−15164.
(60) Chen, K.; Muthukumar, M. Entropic Barrier of Topologically Immobilized DNA in Hydrogels. *Proc. Nat. Acad. Sci. U. S.* **2021**, *118*, No. e2106380118.

https://doi.org/10.1021/acs.jpclett.2c02733
J. Phys. Chem. Lett. 2022, 13, 10612−10620